JOURNAL OF PROPULSION AND POWER
Vol. 21, No. 1, January–February 2005

Downstream Ion Energy Distributions in a Hollow Cathode Ring Cusp Discharge

John E. Foster* and Michael J. Patterson*
NASA John H. Glenn Research Center at Lewis Field, Cleveland, Ohio 44135

The presence of energetic ions produced by a hollow cathodes operating at high-emission currents (>10 A) has been documented in the literature. As part of an ongoing effort to uncover the underlying physics of the formation of these ions, ion efflux from a high-current hollow cathode operating in an ion thruster discharge chamber was investigated. With use of a spherical sector electrostatic energy analyzer located downstream of the discharge cathode, the ion energy distribution over a 0–60-eV energy range was measured. The sensitivity of the ion energy distribution function to zenith angle was also assessed at three different positions: 0, 15, and 25 deg. The measurements suggest that the majority of the ion current at the measuring point falls into the analyzer with an energy approximately equal to the discharge voltage. The ion distribution, however, was found to be quite broad. The high-energy tail of the distribution function tended to grow with increasing discharge current. Sensitivity of the profiles to flow rate at fixed discharge current was also investigated. A simple model is presented that provides a potential mechanism for the production of ions with energies above the discharge voltage.

Nomenclature

a	=	minimum radius of orifice plate channel, m
d	=	distance between electrostatic spherical sector energy analyzer (ESA) and entrance, m
E	=	ion energy, eV
E_n	=	energy acquired after nth bounce, eV
E_0	=	energy of incident ion, eV
E_{01}	=	energy of rebounding particle, eV
e	=	1.6×10^{-19} C
L	=	channel length
l_{cex}	=	charge–exchange mean-free path length, m
l_i	=	electron–neutral ionization path length, m
l_{nn}	=	neutral–neutral mean-free path length, m
M_1	=	mass of incident ion, kg
M_2	=	mass of target material, kg
N	=	minimum number of bounces
n	=	bounce index number
n_e	=	electron number density
R	=	electrostatic energy analyzer mean radius, m
r_1	=	radius of inner sector of electrostatic energy analyzer, m
r_2	=	radius of outer sector of electrostatic energy analyzer, m
U	=	upper level excited state energy, eV
V_c	=	cathode fall voltage, V
V_d	=	discharge voltage, V
V_p	=	plasma potential measured with respect to cathode potential, V
α	=	ratio of mass of incident ion to mass of target
ΔE	=	ESA energy resolution, eV
ΔV	=	potential difference between ESA spherical sectors, V
$\theta_{\max}$	=	maximum rebounding angle, deg
λ_s	=	cathode sheath thickness, m
v_E	=	velocity component parallel to cathode sheath electric field, m/s
v_T	=	random thermal velocity, m/s
ϕ	=	sector angle, deg
φ	=	chamfer angle
ω	=	entrance aperture diameter, m

Presented as Paper 2003-4865 at the AIAA/ASME/SAE/ASEE 39th Joint Propulsion Conference, Huntsville, AL, 20–22 July 2003; received 22 August 2003; revision received 16 September 2004; accepted for publication 31 August 2004.

*Research Engineer, Onboard Propulsion and Power Branch.

Introduction

DEEP space missions utilizing ion thrusters will require very long thrusting times.[1,2] Such long operation times place demanding requirements on the lifetime of thruster components. Components such as the ion optics and the discharge and neutralizer hollow cathodes are continuously subjected to erosion processes driven by ion bombardment via either direct impingement or charge exchange.

Hollow cathodes are subjected to ion bombardment from the surrounding discharge plasma. Additionally, as evidence suggests, under certain conditions, cathodes may be a source of very energetic ions that can drive self-erosive processes as well as the erosion of upstream surfaces such as the screen grid. Indeed it was the erosion of internal discharge chamber structures such as the cathode baffle that led to the first suppositions hinting at the existence of an energetic heavy particle beam emanating from the discharge cathode. In studies led by Mantenieks and Rawlin,[3] Rawlin,[4] and Brophy and Garner[5] severe baffle erosion was observed that was suggestive of energetic ion bombardment. Findings from these studies eventually led to the initiation of research aimed at determining the underlying mechanism for the observed erosion. The bell jar studies of Friedly and Wilbur[6] determined that there were indeed very energetic ions originating at the discharge hollow cathode. These studies indicated that the magnitude of the energetic ion component increases with increasing discharge current. To date, the production of energetic ions in hollow cathode discharges has been documented by a number of studies.[6–12] Theories attempting to describe the production mechanisms of these ions range from the existence of a potential hill,[6,8,10] to magnetohydrodynamic[7] effects to charge–exchange,[9] to hydrodynamic drag driven primarily by electron–ion collisions.[11] To date, however, there has been no satisfactory complete explanation offered for the production of the energetic ions.

The work presented here represents a continuation of ongoing research aimed at fully characterizing ion emission efflux from a high-current hollow cathode.[12] In the present work, the spherical sector electrostatic energy analyzer is used to measure the ion energy distribution as a function of zenith angle relative to the cathode axis as well as discharge cathode flow rate. The study was conducted in a multicusp magnetic environment characteristic of ion thruster operation as described in an earlier work.[12] In this respect the findings are likely representative of ion thruster operation in regards to plasma production mechanisms and in particular

plasma containment by the axial magnetic field in the near-cathode region.[12]

Experimental Setup

The experiments were conducted in a 91 cm long by 48 cm in diameter cryopumped bell jar shown in Fig. 1a. The bell, which was made of Pyrex®, allowed for excellent visual inspection of the discharge as shown in Fig. 1b. The discharge itself was generated using a NASA Evolutionary Xenon Thruster (NEXT) hollow cathode assembly. The cathode assembly included a coaxial keeper electrode assembly that was allowed to float during this investigation. The nominal floating potential over the operating range investigated here was approximately 5 V. The hollow cathode assembly was installed in a 30-cm discharge chamber of similar geometry to that of the NASA Solar Electric Propulsion Technology Application Readiness (NSTAR) thruster. Again, the choice of conducting the investigation of energetic ion efflux using a hollow cathode in a ring cusp discharge chamber was made primarily to determine the nature of the ion efflux in a thrusterlike environment. The magnetic field near the cathode tip was approximately 90 G. For this study, the hollow cathode was operated grounded.

The energy distribution of the ion flux exiting the discharge chamber was characterized using an electrostatic spherical sector energy analyzer (ESA). The ESA was located on axis with the hollow cathode, separated by approximately 23 cm. This experimental setup is shown in Fig. 2. The analyzer consisted of two spherical sectors (141 deg in this case) in which the potential of each relative to ground was varied. The potentials on these surfaces determine the energy that an entering particle must have to pass through from entrance slit to exit slit. In this respect, the ESA can be operated as an energy selector. The energy of the particles that can pass through

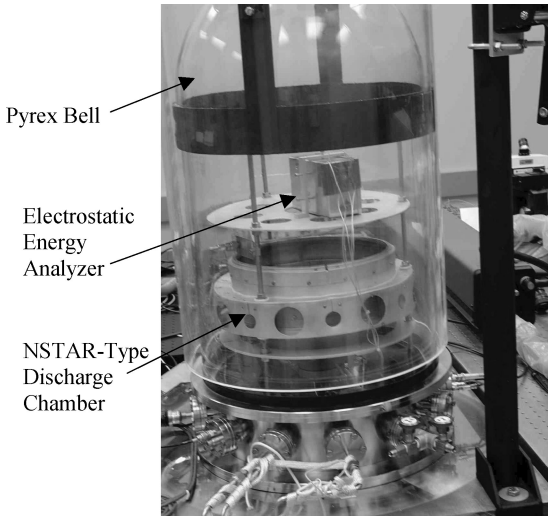

Fig. 1a Bell jar facility and test hardware used for experimental investigation.

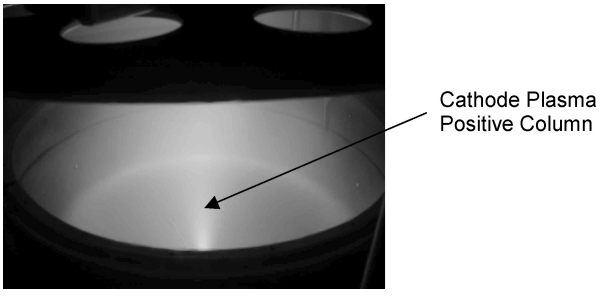

Fig. 1b Visual inspection of discharge operation reveals two distinct plasmas: cathode plasma (plume emanating from cathode) and main discharge plasma, which appears more diffuse and weaker in intensity than cathode column.

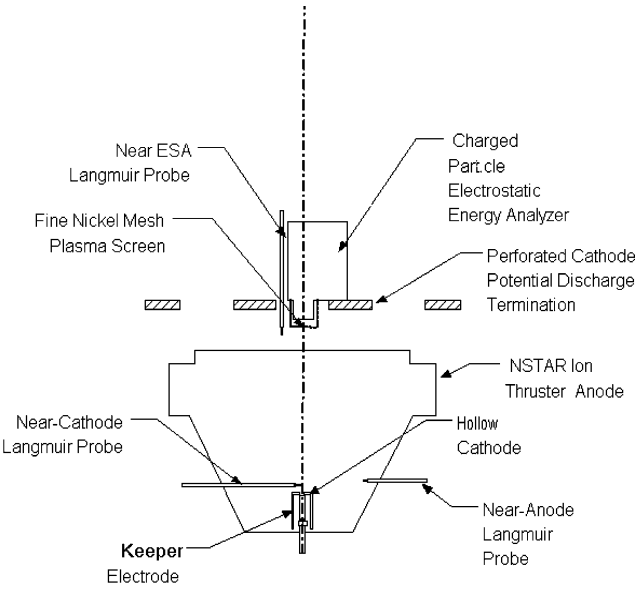

a) Experimental setup

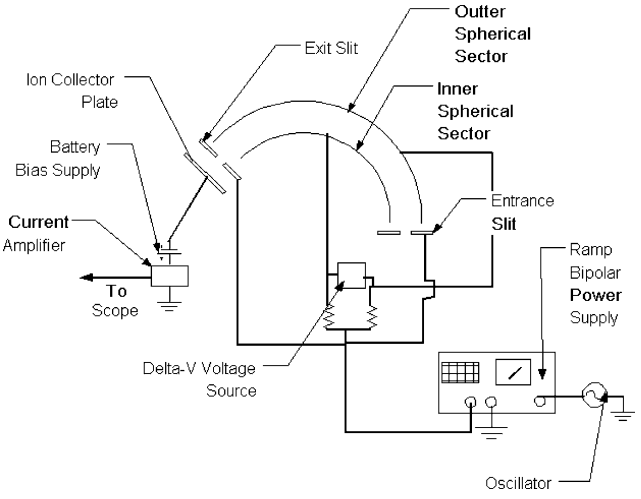

b) ESA bias supplies and data acquisition

Fig. 2 Setup and circuit layout.

can be calculated based on the geometry and potential difference between the spherical surfaces,

$$E = \Delta V/[(r_1/r_2) - (r_2/r_1)] \tag{1}$$

with an energy resolution also determined by geometry and energy,

$$\Delta E/E \approx \omega/[R \cdot (1 - \cos\phi) + d \cdot \sin\phi] \tag{2}$$

The ESA was operated in a constant transmission energy mode. The electrical connections for operation and data acquisition from the ESA is shown in Fig. 2b. The transmission energy as determined by the potential difference between the two spherical surfaces was set at 10 eV. With this transmission energy, the energy resolution was approximately 0.347 eV. The input slit varied in potential so that ions with energies between 0 and approximately 60 eV could be scanned. This mode of operation is similar to that used by Kameyama and Wilbur in their investigation of ion efflux from high-current hollow cathodes.[8] The ESA was housed in an iron box to reduce the effect of the local magnetic field generated by the thruster discharge chamber. The magnetic field at the entrance slit of the ESA was less than 1 G. To minimize the flow of plasma into the device, a cup made of very fine, electroetched nickel was placed over the entrance slit. The mesh makeup was 20 lines/mm with a 0.039-mm spacing between lines. The nickel wire that made up the mesh was 0.01 mm in

diameter. The mesh and the iron box were fixed at ground potential. The electrostatic energy analyzer was suspended over the discharge chamber via a perforated aluminum termination plate. The plate, which was located roughly 8.5 cm downstream of the discharge exit plane, contained eight 9-cm-diam holes and one 8.5-cm-diam center hole. This plate was operated at cathode potential during this investigation.

This open geometry was chosen because of its higher conductivity of neutrals away from the discharge chamber as compared to discharge studies with a simulated grid terminating the exit plane. The open geometry of the test apparatus allows the discharge pressure to be maintained at values similar to that of the bell jar. Because the bell jar pressures are similar to those that prevail in ion thrusters [$\sim$0.013 Pa ($\sim 1 \times 10^{-4}$torr)], the discharge characteristics are expected to be similar to actual ion thruster operation, thereby circumventing issues associated with gridded discharge studies.[13] This notion is supported by the magnitude of the discharge voltages measured during the tests (many of which were similar in magnitude to NSTAR engine operation, $\sim$26 V).

As indicated in Fig. 2b, plasma properties at a select location in the discharge chamber was measured using three cylindrical langmuir probes. The collecting surface of each probe was made of tungsten wire. Two of the probes were located in a plane normal to the discharge axis but located $\sim$3 mm downstream of the cathode keeper. These probes, whose tips were 0.38 mm in diameter and 3 mm long, were used to assess plasma properties in the plane that approximately contained the face of the keeper. One probe was located approximately 2-mm off-axis. The second of the keeper plane probes was located approximately 2 cm above the surface of the anode. In this regard, the probes could be used to determine the average potential difference between these two points. A third probe, 5.5 mm long and 0.38 mm in diameter, was used to measure plasma properties near the entrance slit of the ESA. This probe was located approximately 2 cm below the energy analyzer and approximately 1-cm offaxis of the energy analyzer.

Experimental Results and Discussion

The ion energy distribution was measured as a function of both discharge current at a fixed flow rate and as a function of flow rate at fixed discharge current. For all operating conditions, the bell jar pressure never exceeded 2.0×10^{-2} Pa. Ion energy spectra were collected over a wide discharge current range (8–16 A). Before plasma measurements were taken, the discharge was allowed to stabilize at each operating condition. In all cases, the peak-to-peak oscillations in the discharge voltage were less than 3 V.

Figure 3 shows typical variations in discharge voltage at a fixed flow rate as a function of discharge current over an extended range. The discharge voltage increases linearly with increasing discharge current up to nearly 16 A, at which point the discharge voltage appears to plateau.

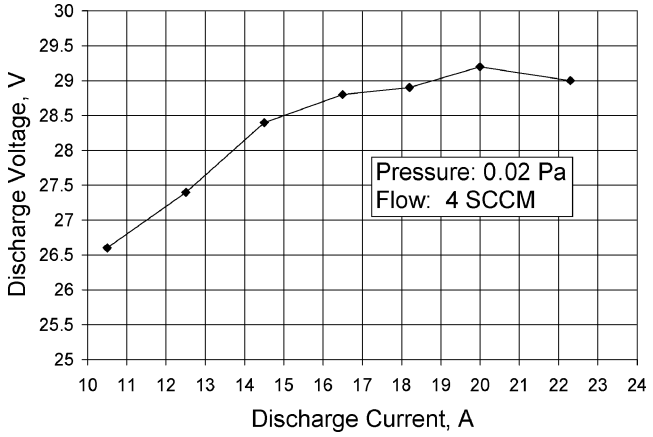

Fig. 3 Discharge characteristics of cathode inside NSTAR discharge chamber at fixed flow rate; discharge voltage uncertainty <1.5 V.

Ion Energy Distribution Measurements

One primary objective of this work was to investigate the possible existence of energetic ions emitted from the hollow cathode. Energetic ion flux produced at or near the discharge cathode should be detectable by the downstream located ESA. The energy range of the investigation was extended to approximately 60 eV. Energies above 60 eV were not investigated because it was found that at the ESA entrance slit bias voltages required to measure this energy range perturbed the plasma. Measurements made at Colorado State University (CSU) suggest that there is an angular dependence to the ion energy distribution function. Indeed, findings from the group indicates that the energetic ions are detectable off-cathode axis.[14] To determine if such phenomena prevails with the 1.27-cm NEXT discharge cathode, ion energy distribution functions were characterized as a function of zenith angle relative to the axis of the discharge cathode.

ESA Zenith Angle = 0 Degrees

Figure 4 shows the variations in the of the ion energy distribution function as at a discharge current of 13.6 A as the flow rate is reduced from 4.3 to 3.5 standard cm^3/min (SCCM). As can be seen in Fig. 4, the peaks are fairly broad and centered near an energy roughly commensurate with the discharge voltage. The location of the central peak was on average approximately 5 eV below that which would be expected of an ion falling through a sheath potential difference comparable to the discharge voltage. This observation is consistent with similar measurements made elsewhere.[8,12] Part of the discrepancy is due to the absolute uncertainty in the discharge voltage, whose peak to peak variations were as much as 1–2 V. The remaining energy discrepancy could be attributed to ions born near the analyzer on a potential plateau that is lower than the plasma potential in the bulk discharge. Langmuir probe measurements made near the analyzer appear to support this notion. The plasma potential measurements made near the analyzer were consistently lower than the discharge voltage by approximately 3–10 V. Figure 5 shows the difference between the plasma potential as measured just downstream of the energy analyzer and the discharge voltage for a number of different discharge currents at 4.3 SCCM.

The broad peaks observed were distributed over a fairly large energy range, with the peak width expanding in energy with increasing flow rate. The variation in the full-width half-maximum (FWHM) increased linearly with increasing flow rate changing from just of 8 eV at 3.5 SCCM to over 13 eV at 4.3 SCCM. This behavior with increasing flow rate (cathode pressure) is attributed to an increase in scattering events. In this regard, it can be characterized as a form of collisional broadening. Such broadening increases the magnitude of the energy distribution ion current signal on both low-energy and higher-energy sides of the peak. At fixed discharge current, the peak intensity also increases with increasing flow rate. The nearly linear increases in peak height with increasing flow rate is consistent with observed increases in plasma density measured just upstream of the analyzer.

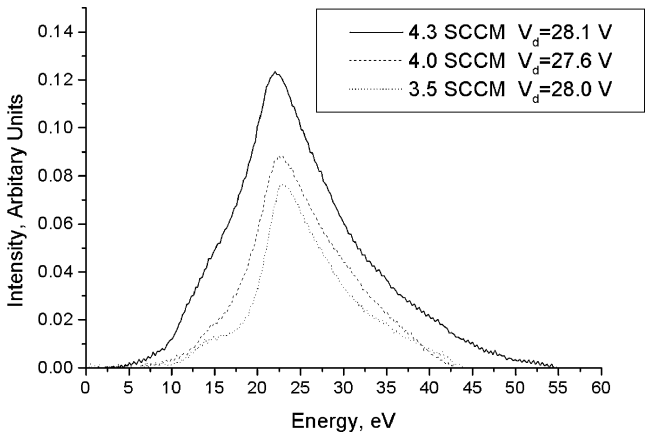

Fig. 4 Variations in the ion energy distribution function with flow rate at fixed discharge current: I = 13.6 A, zenith angle = 0 deg.

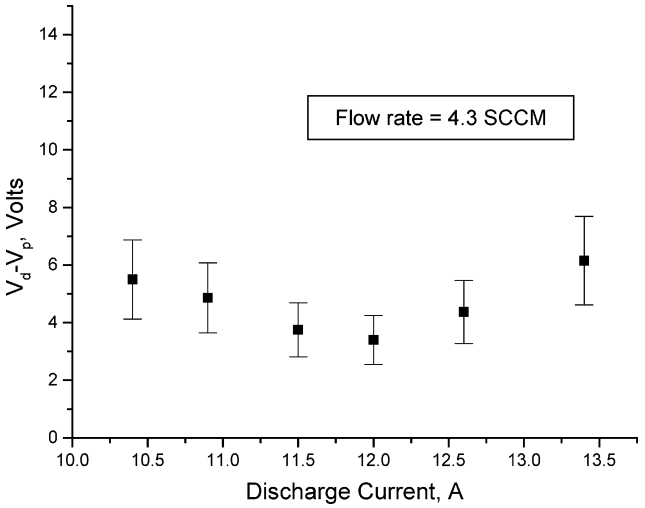

Fig. 5 Variations in difference between peak energy and potential energy of an ion located just downstream of analyzer as inferred from discharge voltage and local plasma potential.

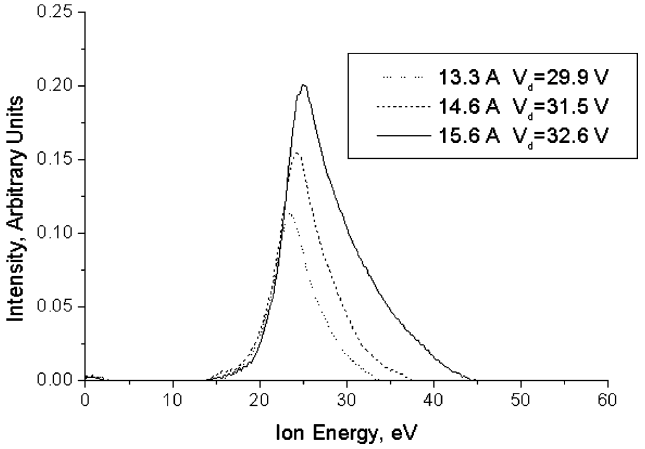

Fig. 6 Variation in ion energy distribution with discharge current at fixed flow: 2 SCCM, zenith angle = 0 deg.

The absolute peak width, as evaluated at the peak baseline, is somewhat puzzling. The fraction of ions making up the distribution function with energies less than the discharge voltage is attributable to charge–exchange ions formed in the region between the analyzer and mesh. This observation is also consistent with similar measurements.[8] On the other hand, the ions with energies well above the discharge voltage potential are not so readily explainable. Though the peaks tended to be centered near energies associated with the discharge voltage, the distribution functions tended to extend 20–30 eV beyond this peak energy. Indeed, at 4.3 SCCM, the wing of the ion energy distribution extended to nearly 60 eV.

As discussed earlier, the peaks tended to narrow and sharpen with decreasing flow rate. Figure 6 shows the behavior of the energy distributions at the reduced xenon flow rate of approximately 2 SCCM as a function of discharge current. The sharpening of the peaks and, particularly, the reduction in distribution intensity at the lower flow rates are likely associated with reduced collisional broadening. In all cases, the location of the distributions' peaks tended to track changes in the discharge voltage. Also, as can be seen in Fig. 6, there is a noticeably sharp rise in intensity on the low-energy side of the distributions. In fact, the sharp rise in intensity occurs at nearly the same energy, just over 22 eV, for all of the curves acquired at this fixed flow rate. This sharp rise is indicative of the magnitude of the potential drop that that exists between the mesh that covers the analyzer and local plasma potential. Indeed, this value of 22 eV is consistent with the plasma potential measurements made just downstream of the analyzer whose average value for these operating conditions was approximately 23.5 V.

With increasing discharge current, the absolute width of the distribution broadened, extending to higher energies, to nearly 25 eV above the discharge voltage The FWHM increased linearly with increasing discharge current, increasing from approximately 5 eV at 13.3 A to nearly 8 eV at 15.6 A. These expansion toward higher energies in the distribution function tail indicate that the population of energetic ions increases with increasing discharge current. The ion signal at all energies increased with increasing discharge current. Indeed, the peak intensity increased linearly with increasing discharge current. This behavior over this limited current range is associated with the measured increases in the plasma density. Note, however, that the population of ions in the tail grows much more rapidly than that at the peak. For example, the ion signal at 33 eV increases exponentially with increasing discharge current. This finding suggests different origins for ions in the tail as opposed to those near the most probable value. The energy distributions taken at fixed currents and fixed flow rates all indicated the presence of energetic ions with energies well in excess of the discharge voltage.

ESA Zenith Angle = 15 Degrees

The angular position of the electrostatic energy analyzer was varied using precision machined wedges as shown in Fig. 7. Ion energy distribution functions taken at different operating conditions at an orientation of 15 deg are shown in Fig. 8. In general, peak intensities at off-axis angles were weaker. This is largely attributed to reductions in plasma density at the ESA. To obtain the desired cant angle, the probe had to be translated radially, in addition to canting

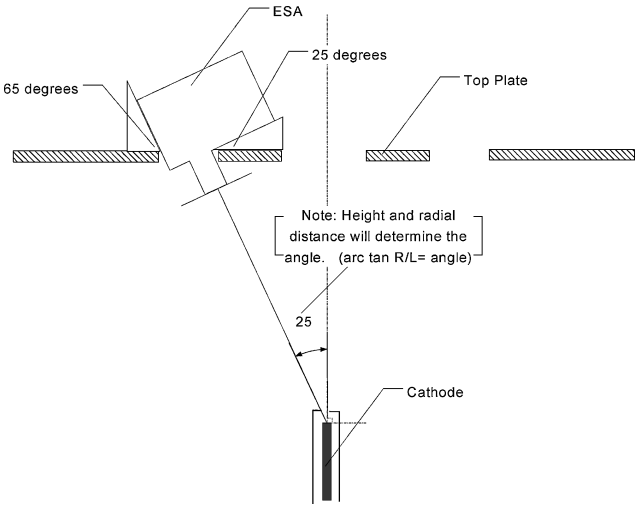

Fig. 7 Use of precision machined wedges to vary angular position of the ESA: 25-deg wedge case.

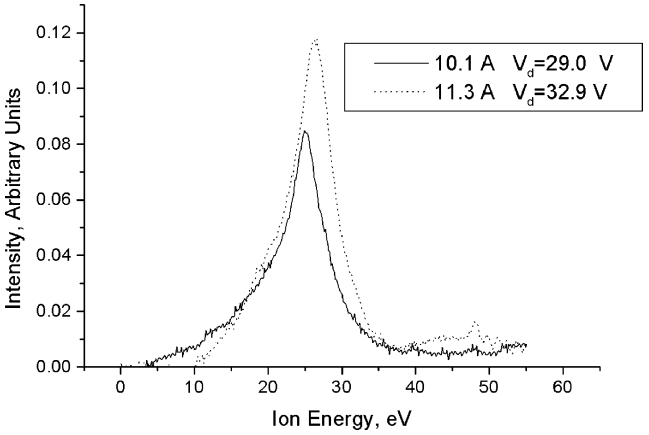

Fig. 8 Variation in ion energy distribution function with discharge current: zenith angle = 15 deg, flow = 2 SCCM.

the analyzer with respect to the input lens axis. Because the discharge is known to be nonuniform (as inferred from beam current density profiles), the plasma density in the region off axis is lower.[15] The radial profile of the ion current density reflects discharge uniformity, which is in general peaked on axis for the NSTAR plasma discharge. The fact that the relative peak intensities were reduced at off-axis locations suggests that, predominantly, the ions falling into the analyzer are primarily from the discharge and are not a well-structured beam propagating from the discharge cathode. As can be seen in Fig. 8, a peak centered near the discharge voltage, which is consistent with the 0-deg orientation cases, again defines the distribution. Additionally, as observed in the 0-deg case, the distributions tended to expand to higher energies with increasing discharge current. The low-energy "shoulder" extended to significantly lower energies than in the 0-deg orientation case. This new feature became more pronounced with increasing angle. The presence of the low-energy shoulder is most likely due to a combination of charge–exchange, scattering within the analyzer, sheath uniformity (or lack thereof) at the analyzer mesh cover, and orientation of the analyzer, which examines the component of the ion falling out of the plasma that is parallel to the analyzer axis itself. Note that, at this orientation, the wings of the ion energy distributions indicate overpopulation relative to what would be expected on a Gaussian distribution, suggesting superthermal ions.

ESA Zenith Angle = 25 Degrees

Examination of spectra taken at a zenith angle of 25 deg possessed additional structure on the low-energy side of the ion distribution, but no additional structure was observed on the high-energy side. As in the 0- and 15-deg case, a primary peak was observed centered near the discharge voltage. These profiles also extended to energies well above the discharge voltage, as indicated in Fig. 9. The presence of distinct peaks other than the central peak, however, was not observed. A more pronounced low-energy shoulder was also observed.

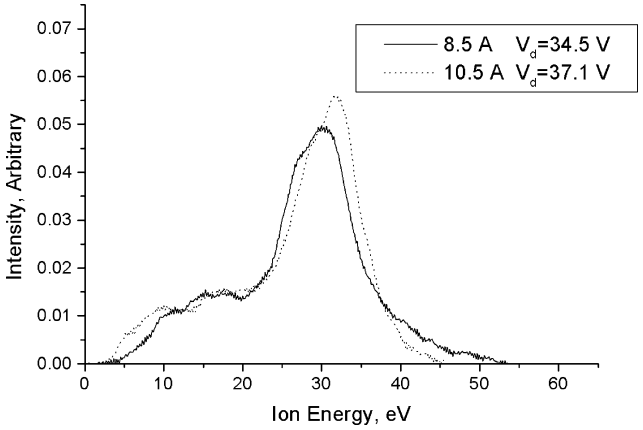

Fig. 9 Variation in ion energy distribution function with discharge current: zenith angle = 25 deg, flow = 1.9 SCCM.

Potential Mechanism for Formation of Energetic Ions

In general, these findings differ from those taken at CSU in that, over the energy range investigated, the presence of distinct, high energetic ion beams emanating from the cathode region was not observed.[14] Instead, energetic ions were only observed in the tail of the distribution function. The energy spread in these largely Gaussian-like profiles can be attributed in part to normal thermal spread in the distribution function. As measured on centerline, the tail extended to higher energies with increasing discharge current or increasing cathode flow rate. The differences between observations in this work and the CSU work initially were attributed to experimental configuration. Early CSU experiments were performed in configurations dissimilar from that of an ion thruster discharge chamber.[6] Recent results, however, indicate that this may not be the case. A more likely reason for the difference may be found in the very nature of the hollow cathode itself. The orifice sizes of the NASA John H. Glenn Research Center (GRC) cathode and the CSU cathode differ significantly. For example, the GRC cathode orifice diameter is significantly larger. As a result, at a given flow rate, internal pressures inside the cathodes are markedly different. The differences in internal pressure environments, which directly effect energy exchange collision processes, also influence the shape of the ion energy distribution function.

Collisional processes inside the cathode can serve as an energy transfer mechanism for the formation of energetic ions. One mechanism for ion energy gain energy arises from collisions taking place within the orifice channel of the discharge cathode. Such processes may contribute to the overpopulated tails observed in the off-axis ion energy distribution functions measured (15 and 25 deg) in this work and that reported in Refs. 8, 9, and 14. Ions produced within the hollow cathode discharge that have velocities directed toward cathode surfaces (barring scattering events) enter the cathode sheath where they are accelerated toward the cathode surface, ultimately attaining an impact energy proportional to the cathode fall voltage: $e \cdot V_c$. The ion on collision with the cathode surface is usually neutralized. A fraction of the ion's incident kinetic energy is converted to thermal energy, which contributes to the maintenance of the cathode temperature. The remaining energy resides as kinetic energy of the rebounding ion or neutral. The fraction of the incident energy that the neutralized ion rebounds with can be described by the following relation[16–19]:

$$\frac{E_1}{E_{01}} = \left(\frac{\cos(\theta) + \sqrt{(M_2/M_1)^2 - (\sin(\theta))^2}}{1 + M_2/M_1} \right)^2 \qquad (3)$$

This relation is derived based on binary collision physics in which momentum and energy are conserved. A schematic of scattering interaction is shown in Fig. 10. According to Eq. (3), the energy

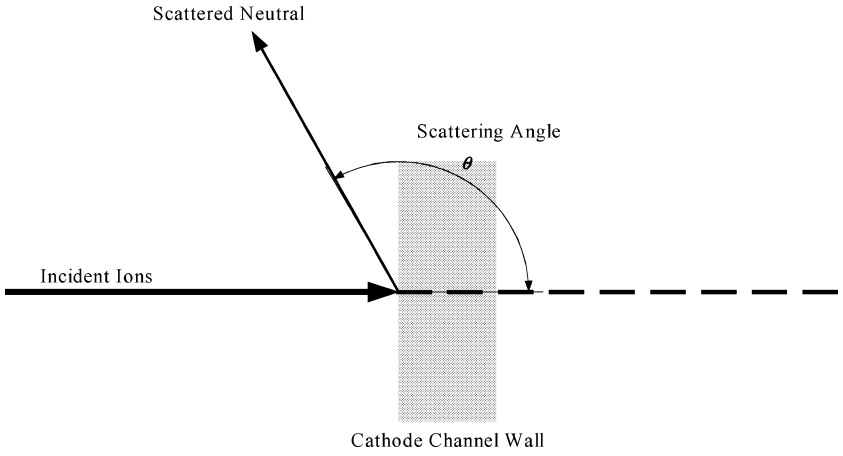

Fig. 10 Relevant scattering geometry with ion rebounding off as a neutral after colliding with cathode channel wall; scattering angle defined relative to ion's incident trajectory vector.

of the scattered particle decreases with increasing angle. Scattered particles with angles nearly parallel to the hollow cathode orifice channel wall rebound with the largest fraction of the incident energy. For normal incidence and specular reflection (where incidence angle equals reflection angle), the scattering angle θ is 180. Equation (3) then reduces to

$$E_{01}/E_0 = (\alpha - 1/\alpha + 1) \tag{3'}$$

where

$$\alpha = M_2/M_1 \tag{4}$$

The fraction of incident energy that rebounding particle leaves the surface increases with α.

When a 180-deg scattering angle is assumed [Eq. (3′)], in the case of xenon plasma within a hollow cathode, incident ions impinging upon the tungsten insert or tungsten orifice plate give rise to an α of approximately 1.4. It then follows from Eq. (3′) that approximately 17% of the incident ion energy leaves as kinetic energy with the neutral, that is, a 25-eV ion, for example, incident on the cathode leaves the cathode surface as a 4.25-eV neutral.

Energetic ions can be generated in the cathode if the ion undergoes multiple impacts with cathode surfaces n times before exiting the cathode. This energy gain mechanism relies on charge–exchange events taking place inside the hollow cathode. Figure 11 shows an exaggerated view of the mechanics of the energy gain process. Here, an ion incident upon the cathode surface leaves the surface as a low-energy neutral. The neutral then proceeds to the opposite cathode surface. Before it reaches the sheath, it undergoes either a charge–exchange collision or an electron impact ionization event where it becomes a low-energy ion still directed toward the cathode surface. The particle then accelerates again, only to rebound from the surface as a neutral once again. However, the resulting neutral is slightly more energetic because the incident ion was also slightly more energetic because of its additional energy from the first impact. The process then repeats itself but is directed at the opposite orifice channel wall. Repeated impacts of this nature give rise to an energy accumulation process in which the ion can exit the cathode at energies greater than the cathode sheath potential. The exit energy of a given ion depends on where the energy gain process began in the orifice channel. This tends to broaden the ion energy spectrum of exiting ions, thereby contributing not only to the spread in ion energy but also contributing to the population of the high-energy tail. Note that this process could give rise to the cathode emission of both energetic ions and neutrals. In the case of the neutrals, the energetic neutral escapes out of the orifice before a charge–exchange collision can take place. These processes could potentially lead to cathode orifice erosion as well, provided that the particles' kinetic energy exceeds the sputtering threshold.[20]

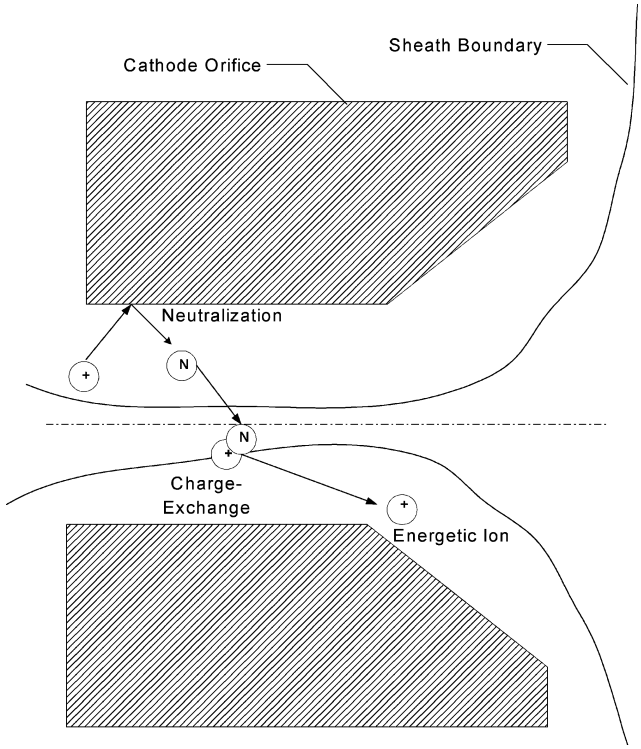

Fig. 11 Energy gain process in cathode orifice channel.

This process of energy gain depends on a number of length scales. Indeed, if the length scales do not satisfy certain conditions, the energy gain process will not be resonant, and thus, the fraction of energetic neutrals and ions generated cannot be expected to be appreciable. The length scales of particular importance include the 1) cathode orifice channel diameter, 2) electron–neutral ionization path length, 3) ion–neutral resonant charge–exchange path length, 4) neutral–neutral collision mean-free path, and 5) cathode sheath thickness. Whether or not these energetic particles form by this mechanism requires that the inequality

$$\lambda_s < l_{\text{cex}} \approx l_i < a < l_{nn} \tag{5}$$

be satisfied. In this respect, this energy gain process is favored if conditions of low pressure and high orifice ionization fractions prevail. For cathode neutral pressures of interest, because the neutral–neutral mean-free path is less than the cathode insert inner diameter, energy gain processes taking place inside the insert are not expected to be significant. The interaction path lengths for all collisions considered were determined based on the relation:

$$l_{\text{cex},i,n} = 1/(N_n \cdot \sigma_{\text{cex},i,n}) \tag{6}$$

The boxed region in Fig. 12 delineates the conditions under which energetic ions can be generated. These operating pressures are typical of thruster discharge cathode operation.[21,22] The relevant mean-free paths are normalized to the cathode orifice diameter. The boxed region is based on an assumed uncertainty of 25% in the cross sections used to calculate the mean-free paths. The ionization fraction in the orifice is taken to be 20% for the data presented in Fig. 12. Over the pressure range associated with this boxed region, the neutral–neutral mean-free path is larger than both the sheath thickness and the charge–exchange path length, making charge–exchange more likely than neutral–neutral scattering. Therefore, charge–exchange events control the charge state that the particle will have when it arrives at the channel wall. In this respect, the rebounding neutral can be converted from ion to neutral to ion again via charge–exchange processes as it moves to the opposite wall. At lower ionization fractions, charge–exchange mean-free paths approach the neutral–neutral mean-free paths making the described energy gain process less likely. This quenching also occurs as pressure increases. As indicated, the boxed region extends from 1 to 10 torr. The energy gain process becomes least likely as the neutral–neutral collision path

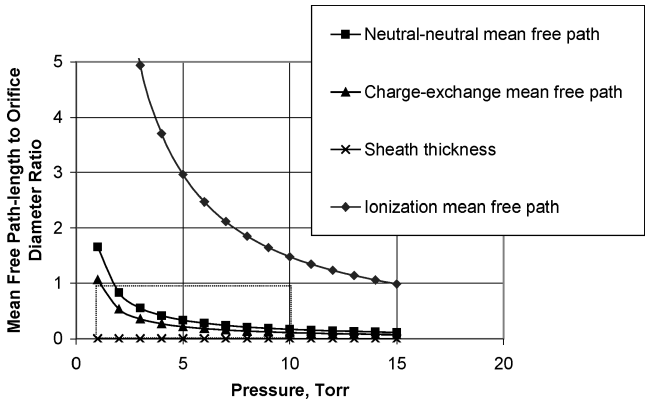

Fig. 12 Relevant mean-free paths over cathode internal pressure range between 0 and 20 torr, regime of interest in box.

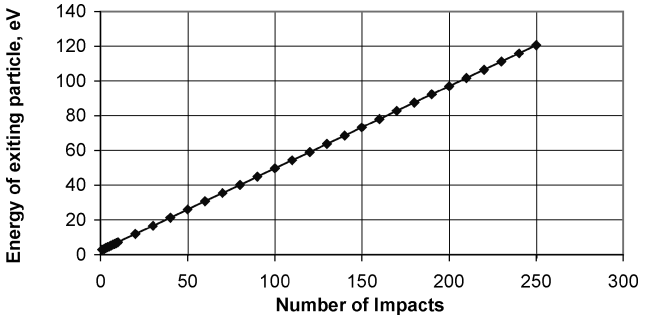

Fig. 13 Variation in energy gain with bounce number, which increases with increasing orifice channel length.

lengths approach the charge–exchange path lengths at pressures beyond 10 torr. Under these conditions, elastic collisions randomize the directed energy and, therefore, quench the process.

The range shown in Fig. 12 is based on the assumption that the distance to the next rebounding surface is along an orifice diameter. In actuality, the particle need not rebound along the diameter. Instead, a rebounding particle can also follow any arbitrary chord to the orifice surface as long as the scattering event is in accord with Eq. (1). In this respect, the actual pressure range over which the energy gain process could possibly extend is beyond the boxed region indicated in Fig. 12.

The energy gain per impact can be determined analytically if specular reflection is assumed. Here, Eq. (3′) applies, and thus, the energy that an ion or neutral can gain during the impacting process increases arithmetically with impact number. The energy of the particle after the nth impact can be determined,

$$E_n = [1 + \gamma \cdot (n - 1)] \cdot V_c \cdot \gamma \tag{7}$$

where γ is the energy attenuation factor defined by the right-hand side of Eq. (3′). This factor depends only on mass ratio. The energy gained by a xenon particle as a function of number of impacts (bounces) within in the orifice channel is shown in Fig. 13. Barring any collisions besides charge–exchange, the xenon particle will oscillate radially between wall surfaces within a plane whose normal is nearly parallel with the axis of the channel. In doing so, with each impact, the particle's energy would increase. Surface texture of the channel, collisions with the particles that make up the ionized gas within the channel, pressure gradients, potential gradients, as well as drift due to small but finite nonradial velocity components associated with the thermal energy of the particle ultimately cause the oscillating particle to "random walk" toward the exit planes of the channel (Fig. 11). The particle trajectory itself may be roughly thought of as a helix as it bounces from side to side traveling along the axis of the cathode toward the channel exit planes.

If it is assumed that the cathode sheath voltage is 17 V, the particle can easily obtain an energy equivalent to the cathode fall voltage provided the channel length is greater than 1 mm (Ref. 21). The observation of the expansion of the ion energy distribution function to higher energies with increasing discharge current could in part be attributed by energetic ion contributions due to this process. In this case, the ionization fraction increases with fixed flow rate and increasing discharge current, which effectively reduces the collisional damping of the charge–exchange process.

Low-Energy Ion Source

The energy gain process described indicates a method by which low-energy ions can be generated. Based on the described processes, a high-fluence low-energy ion source can be developed. Design parameters such as relevant particle interaction mean-free paths, orifice diameter, channel length, gas type, and orifice material type are all important in determining how well such a source will operate. Ideally, the diameter of the orifice channel must be smaller than the neutral–neutral mean-free path to prevent significant randomization of the energy gained after a bounce. Additionally, this diameter must be greater than the charge–exchange or the electron–neutral ionization path length. Maintaining a small neutral–electron ionization mean-free path is difficult at the pressure ranges of interest. In practice, it is much easier for the charge–exchange process to satisfy this condition. Additionally, the orifice channel length can be varied to achieve the desired exit energy. The orifice channel material makeup determines the fraction of energy that the rebounding neutral will leave the surface. In general, the source operates with a higher energy gain per bounce if the mass of the atoms making up the orifice is much larger than that of the incident ions.

Such a low-energy ion source would have practical application in surface analysis areas such as low-energy ion scattering experiments and plasma processing techniques such as surface modification. Additionally, such a source could be used as the basis of a low-thrust, hollow cathode-based propulsion device.

Conclusions

Low-energy ion spectra were acquired at three different zenith angles to characterize the ion emission from a NEXT discharge hollow cathode inside a discharge chamber. The ion spectra appearance was best characterized as broad peaks that tended to extend toward higher energies with increasing discharge current. The distribution functions tended to spread in energy on both the low-energy and high-energy side with increasing flow rate. The data indicate that the dominant ion signal is due to discharge ions falling out of the discharge plasma. Energetic ions were detected only in the tail of the distribution function.

A mechanism for generating energetic ions was proposed. The aim of the model is to explain the energetic ion flux observed in other studies where suitable internal conditions prevail. Energetic ions can be produced by resonant collisions taking place inside the orifice channel. An ion can be generated with appreciable energies due to multiple impacts between cathode surfaces. The conditions that allow such a process to take place depend on key mean-free paths (electron–neutral, neutral–neutral, resonant charge–exchange) relative to the characteristic length scale of the orifice channel and orifice channel ionization fraction. Though a conservative estimate of the energy of the exiting ions can be determined, Monte Carlo or similar computational techniques are necessary to elucidate the details of the phenomenological model. The model presented here points to internal hollow cathode processes that could be exploited in the form of a low-energy ion source. Experimental validation of this model is left to a future investigation.

References

[1]Shotwell, R., "Carbon-Carbon Grid Development for Ion Propulsion Systems," *Proceedings of the 27th International Electric Propulsion Conference*, IEPC Paper 2001-093, Oct. 2001.

[2]Rawlin, V. K., Soulas, G. C., Williams, G. J., and Roman, R. F., "High Specific Impulse, High Power Ion Engine Operation," AIAA Paper 2002-3838, July 2002.

[3]Mantenieks, M. A., and Rawlin, V. K., "Studies of Internal Sputtering in a 30-cm Ion Thruster," *Proceedings of the 11th International Electric Propulsion Conference*, March 1975.

[4]Rawlin, V. K., "Internal Erosion Rates of a 10-kW Xenon Ion Thruster," AIAA Paper 88-2913, July 1988.

[5]Brophy, J. R., and Garner, C. E., "Tests of High Current Hollow Cathodes for Ion Engines," AIAA Paper 88-2913, July 1988.

[6]Friedly, V. J., and Wilbur, P. J., "High Current Hollow Cathode Phenomena," *Journal of Propulsion and Power*, Vol. 8, No. 3, 1992, pp. 635–643.

[7]Latham, P. M., Pearce, A. J., and Bond, R. A., "Erosion Processes in the UK-25 Ion Thruster," *Proceedings of the 22nd International Electric Propulsion Conference*, IEPC Paper 91-096, Oct. 1991.

[8]Kameyama, I., and Wilbur, P. J., "Measurements of Ions from High Current Hollow Cathodes Using Electrostatic Energy Analyzer," *Journal of Propulsion and Power*, Vol. 16, No. 3, 2000, pp. 529–535.

[9]Crofton, M. W., "The Feasibility of Hollow Cathode Ion Thrusters: A Preliminary Characterization," AIAA Paper 2000-5354, July 2000.

[10]Davis, W. D., and Miller, H. C., "Analysis of the Products Emitted by DC Arcs in a Vacuum Ambient," *Journal of Applied Physics*, Vol. 40, No. 5, 1969, pp. 2212–2221.

[11]Hantzsche, E., "A Hydrodynamic Model of Vacuum Arc Plasma," *IEEE Transactions on Plasma Science*, Vol. 20, No. 1, 1992, pp. 34–41.

[12]Foster, J. E., and Patterson, M. J., "Plasma Emission Characteristics from a High Current Hollow Cathode in an Ion Thruster Discharge Chamber," AIAA Paper 2002-24102, 2002.

[13]Brophy, J. R., "Simulated Ion Thruster Operation without Beam Extraction," AIAA Paper 90-2655, 1990.

[14]Farnell, C. C., Williams, J. D., and Wilbur, P. J., "Characteristics of Energetic Ions Emitted from Hollow Cathodes," *Proceedings of the 28th International Electric Propulsion Conference*, IEPC Paper 03-072, 2003.

[15]Foster, J. E., Soulas, G. C., and Patterson, M. J., "Plume and Discharge Plasma Measurements of an NSTAR-Type Ion Thruster," AIAA Paper 2000-3812, 2000.

[16]Smith, D. P., "Scattering of Low-Energy Noble Gas Ions From Metal Surfaces," *Journal of Applied Physics*, Vol. 38, No. 1, 1967, pp. 340–347.

[17]Goff, R. F., and Smith, D. P., "Surface Composition Analysis by Binary Scattering of Noble Gas Ions," *Journal of Vacuum Science and Technology*, Vol. 7, No. 1, 1967, pp. 72–75.

[18]Brongersma, H. H., and Mul, P. M., "Ion Scattering: A Spectroscopic Tool for Study of the Outermost Atomic Layer of a Solid Surface," *Chemical Physics Letters*, Vol. 14, No. 3, 1972, pp. 380–384.

[19]Fauster, T., "Surface Geometry Determination by Large-Angle Ion Scattering," *Vacuum*, Vol. 38, No. 2, 1988, pp. 129–142.

[20]Williams, G. J., "FMT-2 Discharge Cathode Erosion Rate Measurements via LIF," AIAA Paper 2000-3663, 2000.

[21]Salhi, A., Myers, R. M., and Turchi, P. J., "Experimental Investigation of a Hollow Cathode Discharge," *Proceedings of the 23rd International Electric Propulsion Conference*, Paper IEPC 93-025, Sept. 1993.

[22]Goebel, D. M., Jameson, K. K., Watkins, R. M., and Katz, I., "Hollow Cathode and Keeper-Region Plasma Measurements Using Ultra-Fast Miniature Scanning Probes," AIAA Paper 2004-3430, 2004.